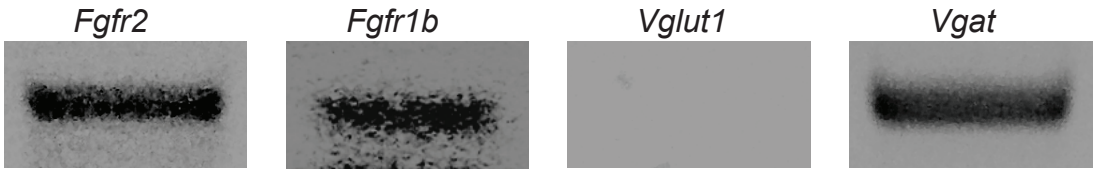

Figure S1. Expression of *Fgfr2* and *Fgfr1b* in CA3 interneurons. Interneurons were isolated using fluorescence-activated cell sorting from the CA3 area dissected from P14 *Vgat-Venus* mice (Wang et al., 2009), followed by mRNA isolation and cDNA synthesis. PCR amplification using specific primers demonstrates the presence of *Fgfr2*, *Fgfr1b*, and *Slc32a1* (*Vgat*) transcripts, but not *Slc17a7* (*Vglut1*) transcripts, in the CA3 interneurons.

Wang, Y., Kakizaki, T., Sakagami, H., Saito, K., Ebihara, S., Kato, M., Hirabayashi, M., Saito, Y., Furuya, N., and Yanagawa, Y. (2009) Fluorescent labeling of both GABAergic and glycinergic neurons in vesicular GABA transporter (VGAT)-Venus transgenic mouse. *Neuroscience* **164**, 1031-1043.

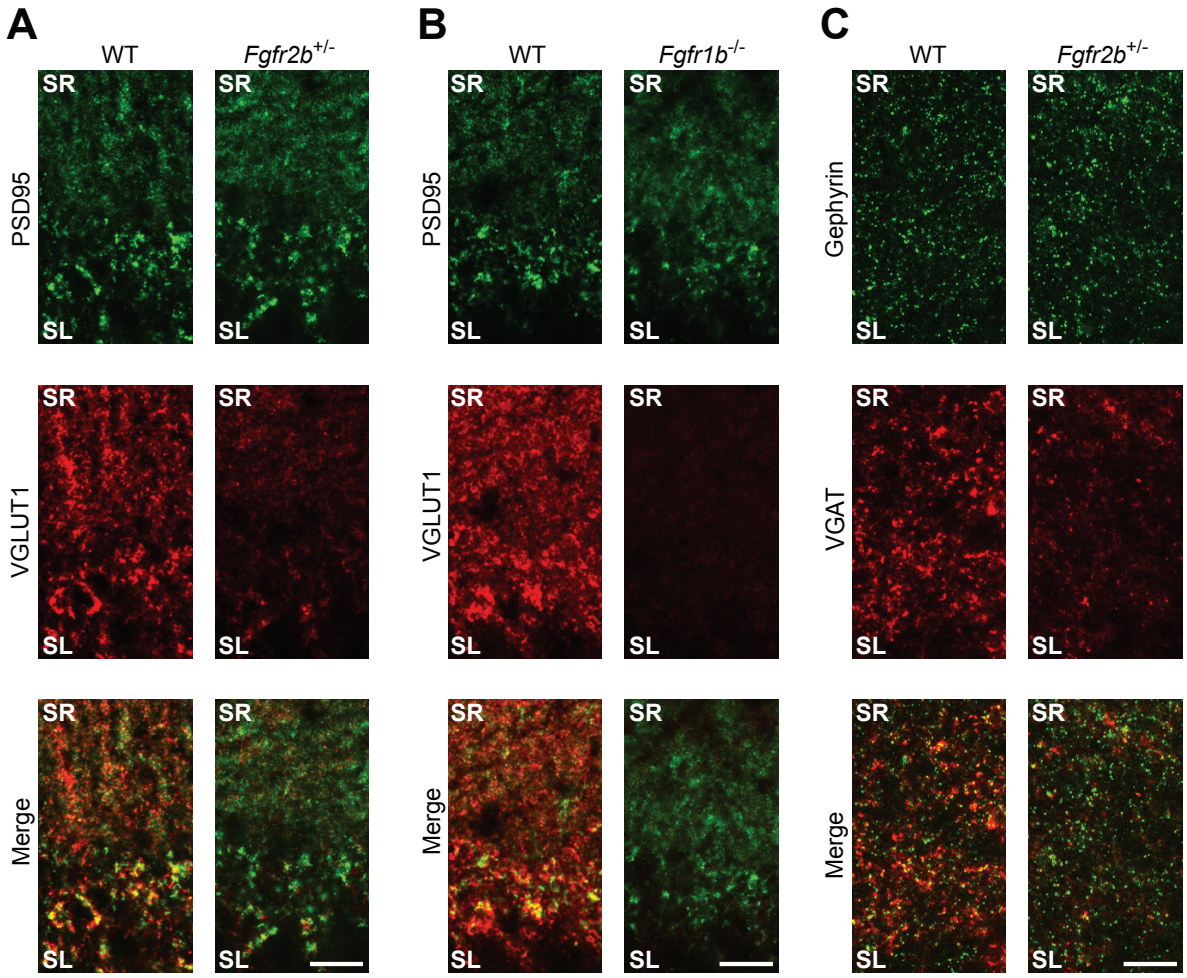

Figure S2. Postsynaptic differentiation is not affected by *Fgfr* deletion. (A) Representative images showing that *Fgfr2b*$^{+/-}$ mice at P8 do not exhibit changes in the clustering of PSD95, a postsynaptic scaffolding protein at excitatory synapses, despite a decrease in VGLUT1 signal. (B) Representative images showing that *Fgfr1b*$^{-/-}$ mice at P8 do not exhibit changes in PSD95 clustering, despite decreased VGLUT1 signal. (C) Representative images showing that *Fgfr2b*$^{+/-}$ mice do not exhibit changes in the clustering of gephyrin, a postsynaptic scaffolding protein at inhibitory synapses, despite decreased VGAT signal. Scale bars, 15 µm.

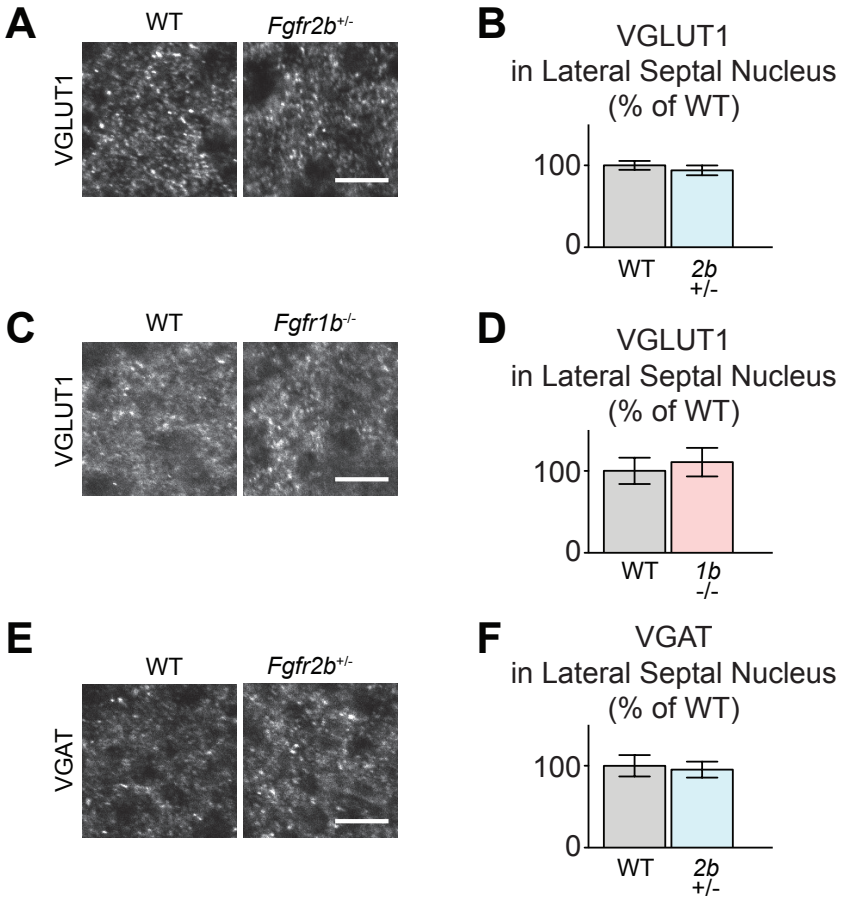

Figure S3. Presynaptic differentiation is not impaired in lateral septal nuclei of *Fgfr*-KO mice. (A-B) *Fgfr2b*$^{+/-}$ mice at P8 have no change in the VGLUT1 staining intensity in the lateral septal nucleus: (A) representative images, (B) quantification of intensity normalized to WT littermates. (C-D) *Fgfr1b*$^{-/-}$ mice at P8 have no change in the VGLUT1 staining intensity in the lateral septal nucleus: (C) representative images, (D) quantification of intensity normalized to WT littermates. (E-F) *Fgfr2b*$^{+/-}$ mice at P8 have no change in the VGAT staining intensity in the lateral septal nucleus: (E) representative images, (F) quantification of intensity normalized to WT littermates. Data represents mean ± s.e.m. Scale bars, 15 μm.

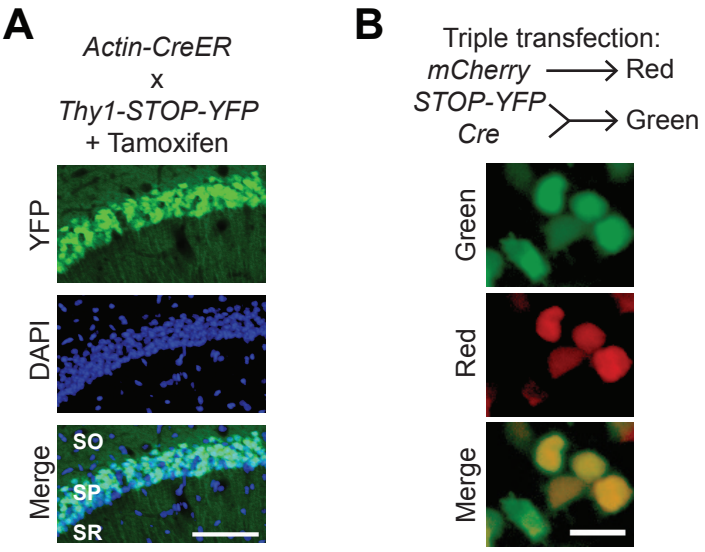

Figure S4. Demonstration of efficient Cre-mediated excision of floxed genes *in vivo* and *in vitro*. (A) Mice carrying the tamoxifen-sensitive Cre (CreER) under a CAG promoter (human CMV virus enhancer and chicken β-actin promoter) (*Actin-CreER*; Guo et al., 2002) were crossed with mice carrying EYFP preceded by a loxP-flanked STOP sequence under a Thy1 promoter (*Thy1-STOP-YFP*; Buffelli et al., 2003). Tamoxifen was injected at P0, activating CreER and leading to expression of EYFP in neurons, with an efficiency of >85%. Representative image of CA1 pyramidal neurons. SO – stratum oriens; SP – stratum pyramidale; SR – stratum radiatum. Scale bar, 100 µm. (B) A Cre expression plasmid was co-transfected with a *loxP-STOP-loxP-YFP* plasmid and an *mCherry* plasmid into HEK cells using calcium-phosphate transfection method. >90% of transfected cells (red) showed Cre-mediated excision of the STOP cassette (green). Scale bar, 50 µm.

Buffelli, M., Burgess, R. W., Feng, G., Lobe, C. G., Lichtman, J. W., and Sanes, J. R. (2003) Genetic evidence that relative synaptic efficacy biases the outcome of synaptic competition. *Nature* **424**, 430-434.

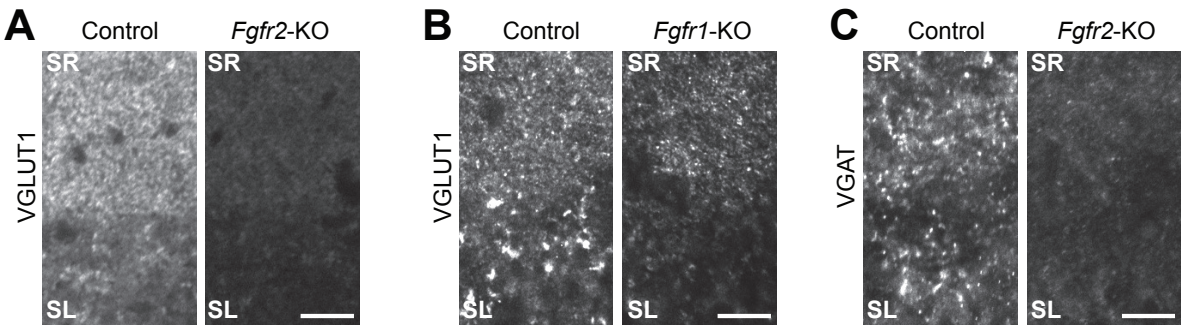

Figure S5. Presynaptic defects persist in the hippocampus of *Fgfr*-KO mice at P14. (A) Representative images showing that defects in VGLUT1 clustering persist at P14 in *Fgfr2*-KO mice. (B) Representative images showing that defects in VGLUT1 clustering persist at P14 in *Fgfr1*-KO mice. (C) Representative images showing that defects in VGAT clustering persist at P14 in *Fgfr2*-KO mice. Scale bars, 15 µm.

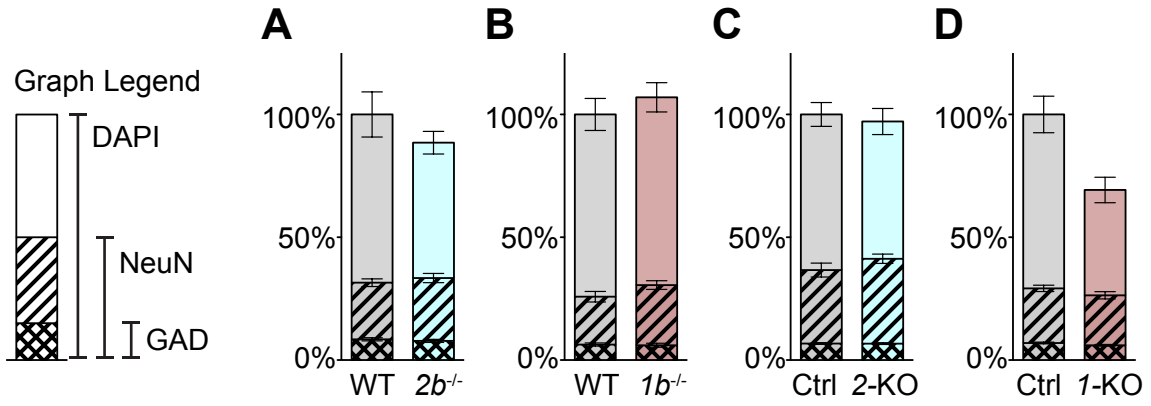

Figure S6. Cell numbers and fates of cultured hippocampal neurons *in vitro*. Cultured hippocampal neurons from WT and *Fgfr2b*$^{-/-}$ mice (A), WT and *Fgfr1b*$^{-/-}$ mice (B), Control and *Fgfr2*-KO mice (C), and Control and *Fgfr1*-KO mice (D) were stained with DAPI to count total cell number, NeuN (1:500, Millipore) to detect mature neurons, and GAD65/67 (1:500, Millipore) to detect inhibitory neurons. Cells were counted from 15 fields (A, B) or 12 fields (C, D) per genotype, each from 3 experiments. No significant changes in the number of total cells, total neurons, or inhibitory neurons were detected between *Fgfr2b*$^{-/-}$, *Fgfr1b*$^{-/-}$, or *Fgfr2*-KO cultures and their respective controls (A, B, C). A significant ($p<0.01$) decrease in the total number of cells, but not total number of neurons or inhibitory neurons, in *Fgfr1*-KO cultures compared to control (D). Cell counts for each set of experiments were normalized to WT or Ctrl DAPI count.

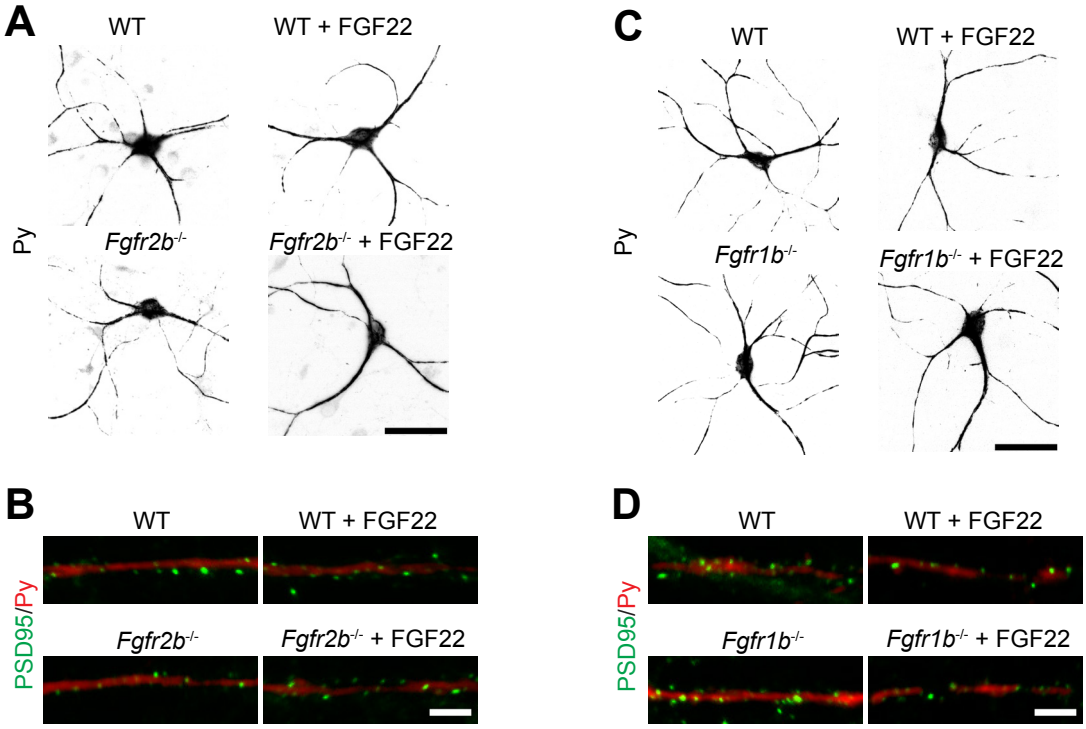

Figure S7. Loss of *Fgfr2b* or *Fgfr1b* as well as application of FGF22 do not lead to apparent changes in dendritic morphology or excitatory postsynaptic differentiation of CA3 neurons. (A) Representative images of WT and *Fgfr2b*$^{-/-}$ neurons with and without FGF22 treatment exhibit similar dendritic morphology, as observed by Py staining in culture. (B) WT and *Fgfr2b*$^{-/-}$ neurons with and without FGF22 treatment do not demonstrate changes in PSD95 (1:500, NeuroMab) staining on Py-positive dendrites. (C) Representative images of WT and *Fgfr1b*$^{-/-}$ neurons with and without FGF22 treatment exhibit similar dendritic morphology, as observed by Py staining in culture. (D) WT and *Fgfr1b*$^{-/-}$ neurons with and without FGF22 treatment do not demonstrate changes in PSD95 staining on Py-positive dendrites. Scale bars in (A, C) are 50 µm. Scale bars in (B, D) are 5 µm.

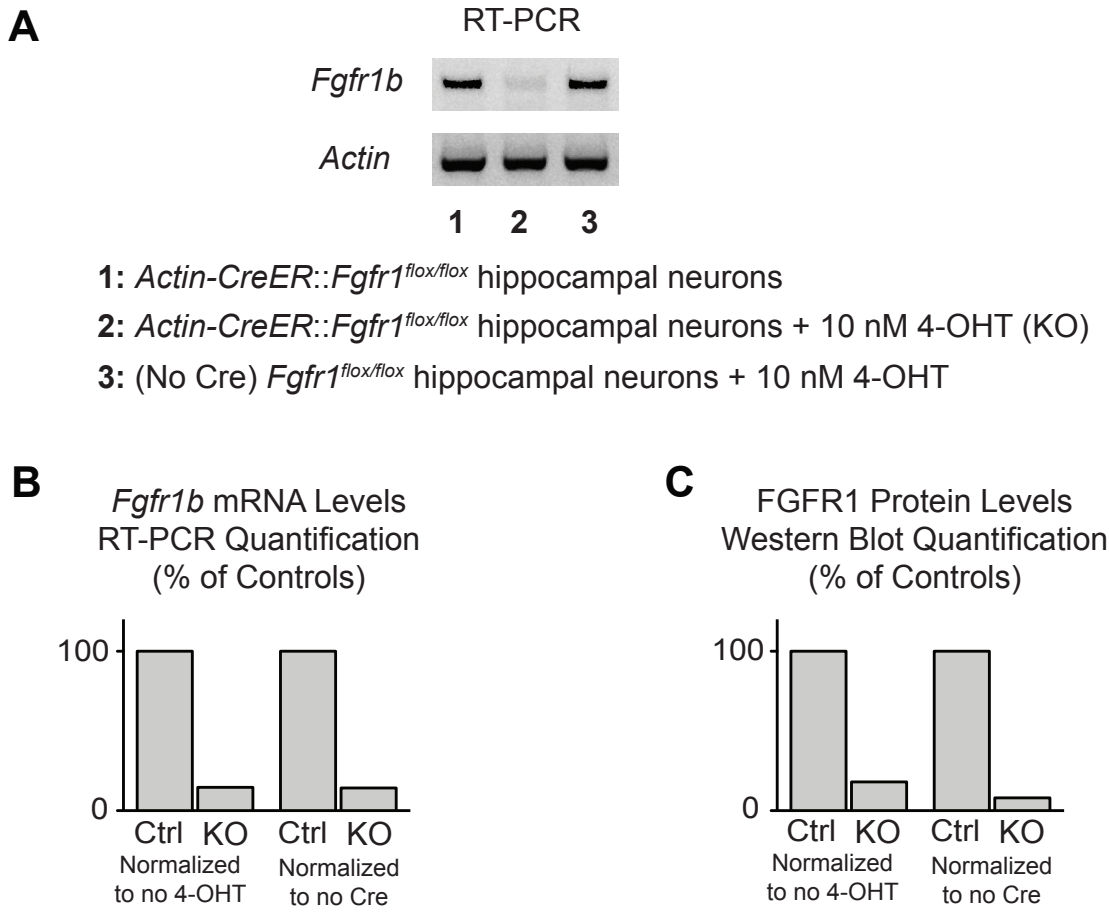

Figure S8. Efficient inactivation of floxed *Fgfr* genes by 4-OH tamoxifen treatment *in vitro.* Hippocampal neuron cultures were prepared from *Actin-CreER*::*Fgfr1*$^{flox/flox}$ and *Fgfr1*$^{flox/flox}$ (no Cre) littermates. Cultures were treated with 10 nM 4-OH tamoxifen (4-OHT). (A) mRNA was isolated and cDNA synthesized from *Actin-CreER*::*Fgfr1*$^{flox/flox}$ not treated with 4-OHT (no 4-OHT control), *Actin-CreER*::*Fgfr1*$^{flox/flox}$ treated with 10 nM 4-OHT at DIV1 (KO), and *Fgfr1*$^{flox/flox}$ treated with 10 nM 4-OHT (no Cre control). RT-PCR using primers specific for *Fgfr1b* revealed a stark decrease in *Fgfr1b* transcripts in KO neurons. (B) Quantification of *Fgfr1b* mRNA levels in KO neurons relative to no 4-OHT and no Cre controls. (C) Quantification of FGFR1 protein levels. KO neurons had a pronounced decrease in the amount of FGFR1 protein compared to no 4-OHT and no Cre controls. Protein lysate was prepared from cultured hippocampal neurons using 50 mM Tris-HCl, 150 mM NaCl, 1% NP-40 lysis buffer supplemented with Protease Inhibitor Cocktail (Roche). Western blot for FGFR1 was performed with the anti-FGFR1 antibody (1:100, Sigma, Cat# F5421). The intensity of FGFR1 bands was quantified with ImageJ.

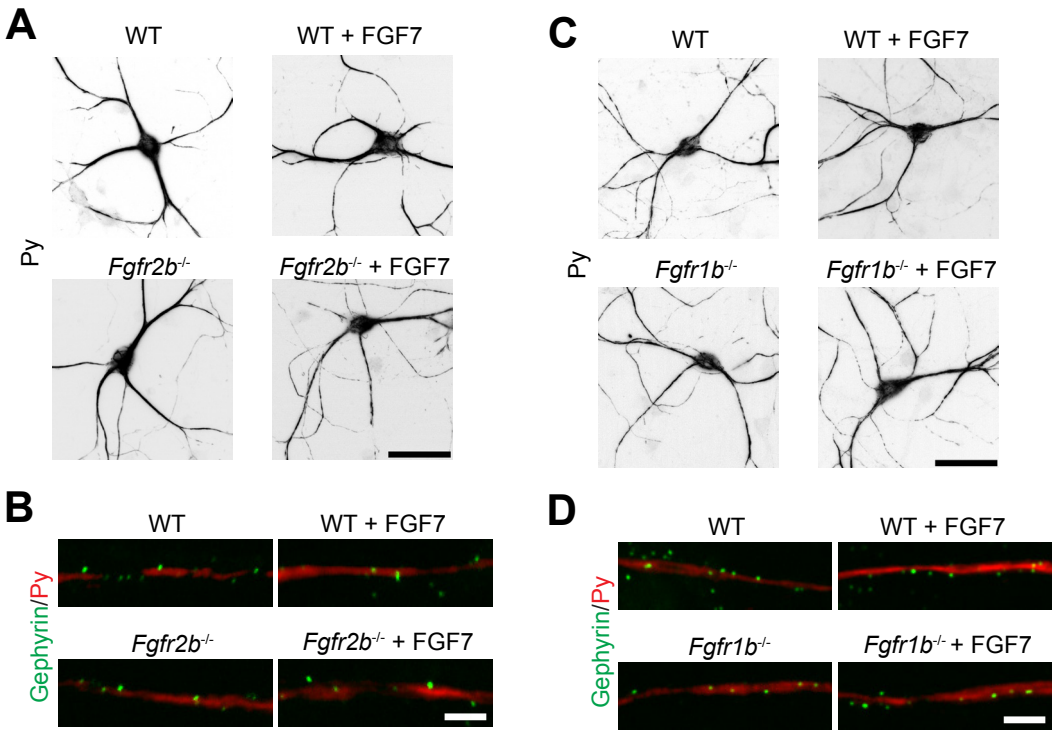

Figure S9. Loss of FGFR2b or FGFR1b as well as application of FGF7 do not lead to apparent changes in dendritic morphology or inhibitory postsynaptic differentiation of CA3 neurons. (A) Representative images of WT and *Fgfr2b*$^{-/-}$ neurons with and without FGF7 treatment exhibit similar dendritic morphology, as observed by Py staining in culture. (B) WT and *Fgfr2b*$^{-/-}$ neurons with and without FGF7 treatment do not demonstrate changes in Gephyrin (1:50, Synaptic Systems) staining on Py-positive dendrites. (C) Representative images of WT and *Fgfr1b*$^{-/-}$ neurons with and without FGF7 treatment exhibit similar dendritic morphology, as observed by Py staining in culture. (D) WT and *Fgfr1b*$^{-/-}$ neurons with and without FGF7 treatment do not demonstrate changes in Gephyrin staining on Py-positive dendrites. Scale bars in (A, C) are 50 μm. Scale bars in (B, D) are 5 μm.

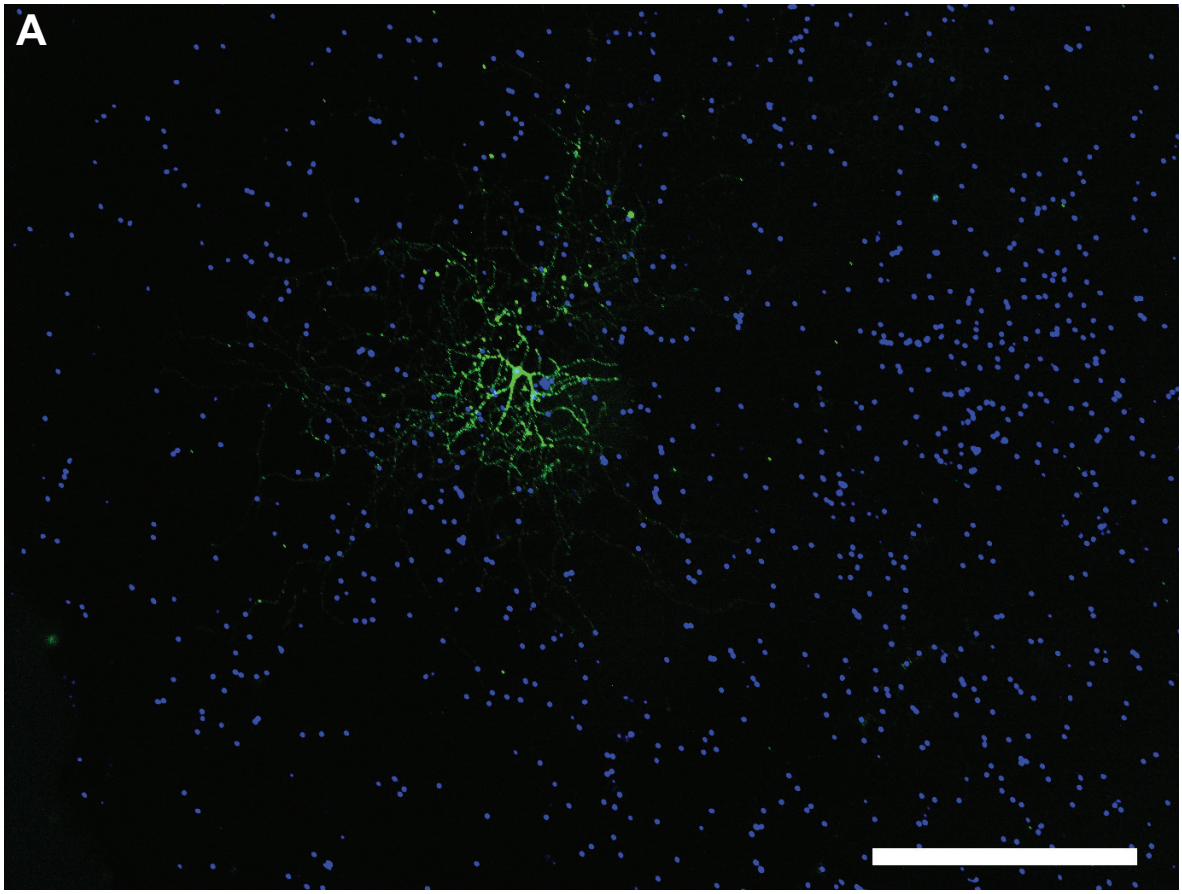

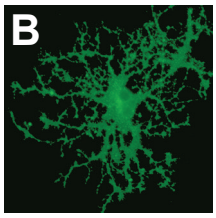

Figure S10. Sparse transfection of synaptophysin-YFP into hippocampal culture.

A) Representative image of a transfected neuron, with punctate synaptophysin-YFP fluorescent labeling (green) of the entire axonal arbor. DAPI (blue) reveals the presence of other untransfected cells. To isolate the effect of transfection for a cell-autonomous effect and minimize the effect of other transfected cells, sparse transfections were performed in experiments described in Figs 9-10. The expression plasmid carrying synaptophysin-YFP under the CMV promoter, together with experimental plasmids (such as Cre expression or empty vector), were transfected into neuronal cultures. Of the approximately 50,000 cells plated on a 12-mm coverslip (113 mm^2), only about 50 cells were transfected per coverslip, thus there were fewer than 0.5 transfected cells per mm^2. Only transfected neurons not contacting other transfected cells were analyzed, to maximize the possibility of cell-autonomous effects. Scale bar, 500 μm.

B) Example image of a synaptophysin-YFP transfected astrocyte. Most transfected cells were neurons and not astrocytes (less than 5% of transfected cells were astrocytes).

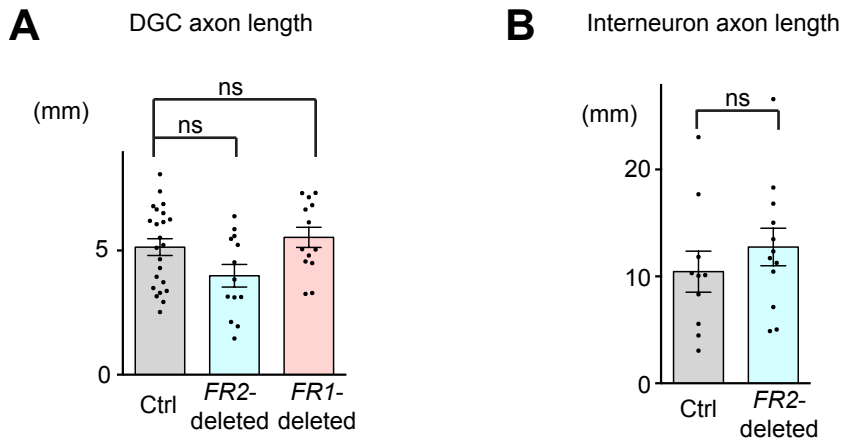

Figure S11. Axon length does not significantly change in *Fgfr*-deleted DGCs or interneurons. (A) Average axon length in *Fgfr2*-deleted or *Fgfr1*-deleted DGCs does not significantly change from control. (B) Average axon length in *Fgfr2*-deleted interneurons does not significantly change from control. Data represents mean ± s.e.m. DGC axon lengths were compared using a One-way ANOVA with a post hoc Tukey's test. Interneuron axon lengths were compared using a Student's t-test. "ns", not significant.